Dynamical double full Bloch beam created with polariton vortices

Lorenzo Dominici (lorenzo.dominici@nanotec.cnr.it)
CNR NANOTEC, Institute of Nanotechnology

Nina Voronova
National Research Nuclear University MEPhI (Moscow Engineering Physics Institute)
https://orcid.org/0000-0001-7419-8820

Amir Rahmani
Azarbaijan Shahid Madani University https://orcid.org/0000-0002-7907-7160

david colas
University of Queensland

Dario Ballarini
CNR-NANOTEC

Milena De Giorgi
CNR NANOTEC - Institute of Nanotechnology https://orcid.org/0000-0002-4522-7933

Giuseppe Gigli
Istituto di nanotecnologia del CNR, Università del Salento

Fabrice Laussy
University of Wolverhampton https://orcid.org/0000-0002-1070-7128

Daniele Sanvitto
National Research Council

Article

Keywords:

Posted Date: February 18th, 2022

DOI: https://doi.org/10.21203/rs.3.rs-1319176/v1

Dynamical double full Bloch beam created with polariton vortices

Lorenzo Dominici,[1,*] Nina Voronova,[2,3,†] Amir Rahmani,[4] David Colas,[5] Dario Ballarini,[1] Milena De Giorgi,[1] Giuseppe Gigli,[1] Fabrice P. Laussy,[3,6] and Daniele Sanvitto[1,7]

[1] *CNR NANOTEC, Istituto di Nanotecnologia, Via Monteroni, 73100 Lecce, Italy*
[2] *National Research Nuclear University MEPhI (Moscow Engineering Physics Institute), 115409 Moscow, Russia*
[3] *Russian Quantum Center, Skolkovo innovation city, 121205 Moscow, Russia*
[4] *Department of Physics, Azarbaijan Shahid Madani University, Tabriz, Iran*
[5] *Aix Marseille Université, CNRS, Centrale Marseille, LMA UMR 7031, Marseille, France*
[6] *Faculty of Science and Engineering, University of Wolverhampton, Wulfruna Street, WV1 1LY, UK*
[7] *INFN sezione di Lecce, 73100 Lecce, Italy*

Abstract. Vortices provide elementary quanta of rotation in superfluids, superconductors, and optics. In the latter case, such vortices are relevant to the encoding of arbitrary quantized angular momentum for both fiber and free-air communications, data elaboration, gyroscopes, and medical tools, and play a prominent role as building blocks in the field of structured light. Differently from the synthetic generation of arbitrary wave shaping, here we exploit the natural assets of open-dissipative exciton-polariton fluids to set into ultrafast motion a doubly-charged vortex, which also results in the time-varying orbital angular momentum of emitted light. The created topology comprises all the possible polariton pseudospins, with each state appearing twice in real space where the Bloch sphere is conformally mapped, with the orthogonality between the parallels and meridians preserved. The density of the sphere metric lines is described by the Berry curvature which is reshaping in time, but always keeps a space integral of twice the solid angle. This confirms that the spiraling motion of the two observable photonic vortex cores is due to the creation of a dynamical full Bloch beam and its evolving metric.

QUANTIZED vortices embody the fundamental aspects of circular motion in all fields and fluids which can be described by an oscillating wavefunction. The complex-valued nature of the wavefunction implies an integer number of phase winding, or wave crests, around the core of such a vortex, related to the quantized value of orbital angular momentum (OAM) per particle. Differently from classical rigid rotations, the rotating quantum fluid assumes a larger momentum and velocity closer to the rotation core, such as in a gavitational orbital motion. An isolated Bose-Einstein condensate rotating around a single or multiply charged central vortex can be thought of as fundamental gyroscope[1], candidating them as sensitive detectors for gravitational waves when implemented in orbiting laboratory[2]. At different levels, analogies were drawn, both in the past and recently, to point-like atoms[3,4] or other elementary particles dressed with at least two quantum numbers and capable of tunable pair-wise interactions[5,6]. Quantum vortices have been mostly studied when dealing with nonlinear fluids and their phase transitions, relevant in their observed macroscopic degree of coherence, in quasi-two-dimensional (2D) as well as in three-dimensional (3D) fields, giving rise to vortex tubes, networks, rings and even knots[7,8]. These entities are called wave dislocations[9] or topological defects, because the phase singularity at their core and the order parameter winding around it are at the very basis of many structured objects of nontrivial geometry. When implemented in photonics, vortices are employed as a further degree of data enconding and for free-air transmission[10–12] as well as for many optical tweezers applications[13] and structured light schemes[14,15]. Further dressed with the spin angular momentum (SAM) or polarization degree of freedom, they can create complex textures around their core[16], subtending 2D and even 3D skyrmions[17], eventually evolving in time[18] thanks to different interactions with a material medium. These objects can be also viewed as full Poincaré[19] or full Bloch beams[20], highlighting their link with deeper mathematical and topological entities and counter-intuitive physical concepts such as time-varying OAM.

Here we study the double full Bloch beam evolution[20] created by a multiple topological charge (or number of singly-charged vortices) initially imprinted by the optical excitation beam and hence transferred to the initial polariton profile, resulting in the spiraling vortex effect. Microcavity polaritons are hybrid light-matter modes resulting from the strong coupling of microcavity (MC) photons and quantum well (QW) excitons. They represent a strong test bed for many quantum fluids phenomena[21] spanning from Bose-Einstein condensation (BEC), long range order coherence, phase transitions[22] and superfluidity, as well as nonlinear and spontaneous or imprinted vortex structures and dynamics[23]. Their open-dissipative nature allows for both the resonant excitation by means of continuous-wave or pulsed laser light, as well as for detection of their state thanks to the emitted light. In the present setting, the double vortex is imprinted by a pulse and perturbed by a second (vortex-free) pulse to achieve the initial state. Its evolution is imaged by means of a digital off-axis holography scheme[24] allowing to retrieve both the amplitude and phase maps of the emission during time. The observed dynamics are obtained thanks to the natural assets of the coupled and open-dissipative polaritons, such as their Rabi oscillations[24] and the difference in decay rates

* lorenzo.dominici@nanotec.cnr.it; https://polaritonics.nanotec.cnr.it/
† nsvoronova@mephi.ru

of the two normal modes (upper and lower polariton modes, UP and LP). In fact, the motion of the photonic vortices can be ascribed to the spatially varying relative phase between the normal modes of the system and their time beating due to their different frequencies. Most importantly, this underlying texture and its dynamics can be described in terms of the pseudospin for the polariton state, mapped by the Bloch sphere metric in real space. This offers the possibility to create and look at a non trivial topology, representing an asymmetric yet conformal double full Bloch beam and its evolution in time.

Polariton double vortex

By means of a q-plate carrying a double topological charge, we shape the photonic pulse A into a modified Laguerre-Gauss LG_{02} state[6]. Its winding ($l_A = 2$) is translated into two unitary co-winding vortices, whose initial separation can be controlled by the tuning of the q-plate device. We exploit this effect to realize a polariton fluid with two spatially separated phase singularities, introducing the potentiality for an asymmetry factor with respect to the following dynamics. After the first pulse, the vortex cores are stably located in the inner region of the spot, split by about 12 μm along an oblique direction (*i.e.*, they are off-axis with respect to the center of the beam), as shown in the bottom maps of Fig. 1a,b reporting the amplitude (a) and phase (b) of the double vortex state at the time of $t = 2.0$ ps, before the arrival of the second pulse B (which is plain Gaussian, $l_B = 0$). Upon the overlap with the pulse B, the vortices are moved further away in opposite directions and reach a maximum distance of ≈ 40 μm (at $t = 2.32$ ps), starting a rotational motion both in clockwise direction, ascribed to their same topological charge. They reach a horizontal alignment ($t = 2.56$ ps) before coming back to the central region after one Rabi-oscillation period, which is shown in the top panels ($t = 2.80$ ps). Their trajectories, extended into the next Rabi period ($t = 2.0$ – 3.6 ps), are reported as superimposed solid lines (red and blue). In summary, the two xyt vortex lines start spiraling into two new positions, and this can be clearly seen when reporting them as a 3D perspective in Fig. 1c.

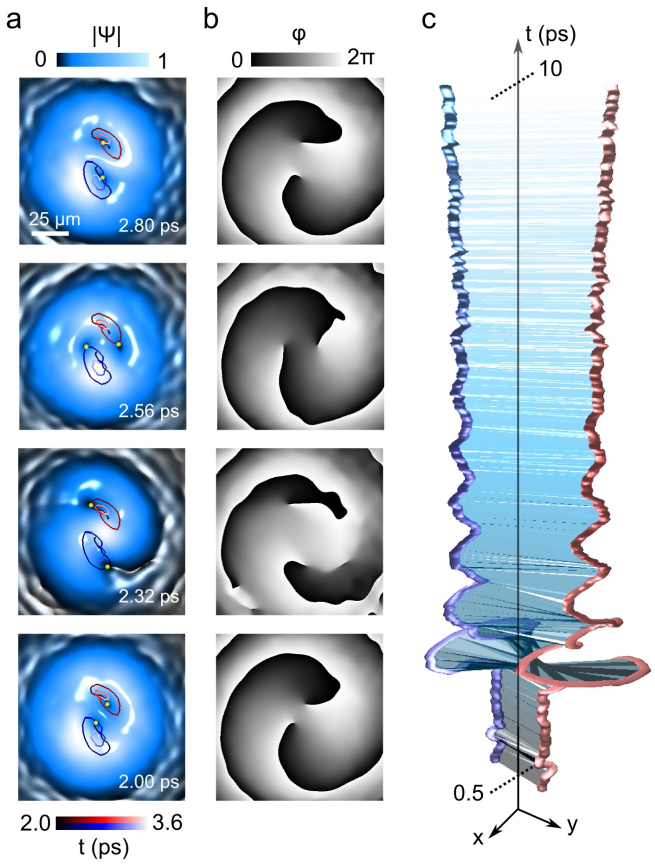

Fig. 1. Double Rabi spiraling vortex. a,**b**, Experimental amplitude and phase maps of the photonic emission from the polariton fluid, when exciting with a double vortex ($l_A = 2$) and after arrival of the control pulse ($l_B = 0$). The different frames correspond to time of $t = 2.0, 2.32, 2.56$ and 2.80 ps. The instantaneous phase singularities are tracked as yellow dots in the amplitude maps, and the solid lines represent the vortex trajectories integrated over two Rabi-oscillations periods ($t = 2.0 - 3.6$ ps, red and blue lines are used to distinguish the two different cores). **c**, Vortex lines plotted as xyt curves (time range $t = 0.5 - 10$ ps, step $\delta t = 0.02$ ps). See also the Supplementary movie SM1.

Phase control

It is possible to perform a fine control of the vortex trajectories upon tuning of the optical phase delay φ_{AB} between the pulses A and B. Figure 2a shows the emitted photon density at a fixed time of the previous dynamics ($t = 3.7$ ps), but for different φ_{AB} spaced by equal intervals of $\pi/4$ (corresponding to $\lambda/8$ steps in the physical delay line for the second pulse). Both vortices describe the same circle (black/white line) when sweeping the phase delay, exchanging their positions when changing φ_{AB} along a $\lambda/2$ length. Although the distribution of the polariton fluid and the positions of the vortex cores look as invariant through such a change, nevertheless, the two vortices can be distinguished by the continuity of their positions. The topological bottle surface in the xyt space described by the double vortex strings is shown in Fig. 2b, in the time range of one and a half Rabi-oscillations period ($t = 2.5$ – 3.7 ps). Here the solid spheres represent the position of the two phase singularities, tracked at time intervals of $t = 0.1$ ps ($t = 0.05$ ps in the last part) and sweeping φ_{AB} at $\pi/4$ steps. The red and blue solid tubes are the specific vortex lines associated to a fixed phase delay (that of the previous figure, sampled with $\delta t = 0.02$ ps), climbing on the surface. Such a topological surface produces a self-twisting "double bottle". It appears to have a cylindrical symmetry, but in reality, two different topologies are observed, which can be revealed by plotting the isotime vortex lines in the virtual $xy\varphi_{AB}$ space. Indeed, when the distance between the two vortex cores is high (large radius of the surface),

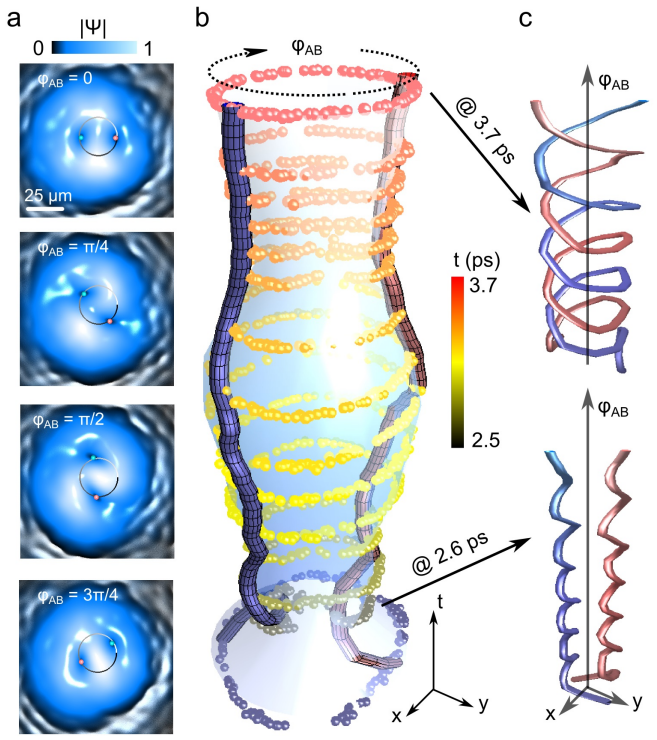

Fig. 2. **Phase delay control of vortex lines. a** Polariton amplitude maps in the double vortex experiment. The snapshots are taken at $t = 3.7$ ps, with four different phase delays φ_{AB} spaced by $\pi/4$. The phase singularities have been marked with blue/red dots in the amplitude maps, and the black/white line is the circle fitting their positions. **b** The specific xyt vortex lines (at a given phase delay) of the two unitary vortices (blue and red tubes) during one and half Rabi-oscillations period (time range $t = 2.5 - 3.7$ ps). The topological bottle surface described by the vortex cores when sweeping the optical phase delay between the two pulses has been mapped (by spheres) at 100 fs or 50 fs time intervals, spanning φ_{AB} in a 15π range by successive $\lambda/8$ steps. **c** Isotime vortex lines described when changing φ_{AB}. Top and bottom panels correspond to $t = 3.7$ ps and $t = 2.6$ ps, respectively.

as at later times, the optical phase scan shows a double helix trajectory around a common center. This is the most prevalent situation, as illustrated in Fig. 2c, top panel (relative to the time $t = 3.7$ ps). Interestingly, when the relative distance between vortices is at a minimum, the trajectories become not intertwined, and each vortex follows a helix trajectory around different centers, as in Fig. 2c, bottom (at $t = 2.6$ ps).

Asymmetry in phase scan

This asymmetry can be understood as an anisotropy factor given by the initial splitting of the two vortices, when compared to the displacement induced by the pulse B. Hence, there is a nodal string of the topological bottle (intersection with a fixed t plane), where the double concentric cylinder undergoes a metamorphosis into two non-concentric and separated quasi-cylinders: the projection of such $xy\varphi_{AB}$ nodal string onto the xy–plane

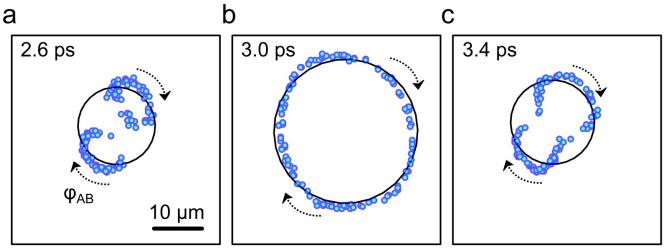

Fig. 3. **Broken symmetry in phase delay scan. a,b,c** Blue points represent the positions of photonic vortex cores in real space at fixed times, when scanning the phase delay between the excitation and control beams as in Fig. 2. At the times when the photon vortex cores are more distant from the centre (e.g., t = 3.0 ps), the phase scan makes their positions rotate with central symmetry, overlapping the fitting circle (black solid line). When the cores are closer to the centre (*e.g.*, t = 2.6 and 3.4 ps), the phase scan makes them describe two ellipses which do not overlap anymore with the fitting circle, but compose a 8-shaped line.

is a 8-shaped line (see also Ref.[25]). The two different situations are represented in Fig. 3, where the circular symmetry is present at given times (*e.g.*, t = 3.0 ps), while the 8-shape is visible at $T_R/2$ time interval from the former (*e.g.*, at t = 2.6 ps and 3.4 ps). Such two situations hence correspond to the times of the Rabi cycles when the twin cores are further from or closer to the centre, respectively.

Local oscillations and underlying texture

In order to model and discuss the observed spiraling, we first retrieve the topological texture underlying to the structured vortex dynamics. Figure 4a shows that the time oscillations of photonic density in a given spatial point can be fitted by the coupled oscillators model. The bare photon and exciton modes have given rise to the UP and LP normal modes, that can be thought as two independent sources now, interfering in the observable photon field. The two normal modes are both differently decaying in time and undergoing a phase change with different frequencies. This evolution can be described by introducing a complex frequency $\omega_{U,L} - i\gamma_{U,L}$. The fitting of photonic emission allows to retrieve this way the spatial maps of the relative phase and amplitude of the two normal modes. The spatial relative phase $\varphi_{LU}(x, y) = \varphi_U - \varphi_L$ has the shape of a quadrupole shown in Fig. 4b, because of the displaced position of the two phase singularities (imprinted by the double-pulse excitation) in each of the normal modes. The two photon vortex cores are moving in round orbits around the relative phase singularities, in the specific case those corresponding to the LP cores. The local polariton imbalance is mapped by a parameter defined as $s(x, y) = (|\psi_U|^2 - |\psi_L|^2)/(|\psi_U|^2 + |\psi_L|^2) = \cos\theta$ which, when shown on the polariton Bloch sphere, is the analogue to the s_3 parameter on the Poincaré sphere. Indeed, θ represents the polar angle of a given

polariton state marked on the Bloch sphere, while φ_{LU} is directly the azimuthal angle of the sphere. Analogously to the Poincaré sphere for the polarizations[26], here the north and south poles of the Bloch sphere for polaritons correspond to the pure UP and LP normal modes (that are spatially positioned in the centre of the vortex of the opposite mode), whereas the equator represents all possible dynamical states of a pure photon or exciton, which are continuosly transforming into each other at the Rabi frequency. The $s(x, y)$ map at $t = 2.7$ ps is shown in Fig. 4c. It is fundamental that the two photon cores, being a zero of the photon intensity, can be understood in terms of a destructive interference between the UP and LP modes, and hence they have to move along the orbit corresponding to $s = 0$. The fitted orbits (white loops in the panel c) fail to precisely retrieve the observed trajectories (red and blue lines), because of the high sensitivity in the weak density areas close to the LP/UP cores, but the agreement is qualitatively good. While the photonic cores move along the orbits due to the relative phase continuous drift in time $\varphi_{LU} = \varphi^0_{LU} + \Omega_R$ (where $\Omega_R = \omega_U - \omega_L$ is the Rabi frequency), the orbits themselves shrink due to the differential decay between the normal modes $\gamma_{LU} = \gamma_U - \gamma_L$.

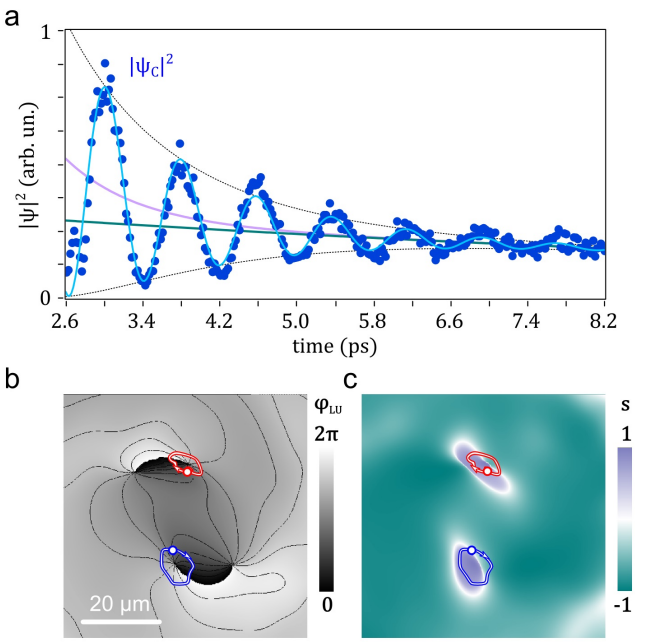

Fig. 4. Oscillations and relative phase and amplitude maps. **a**, Photonic oscillations at a specific point are fitted by the two sources interference model. The procedure allows to retrieve the intensities of the two normal modes in time (solid purple and green lines for the UP and LP modes, respectively) and their relative phase. Repeating the procedure all along the spatial domain allows to plot their 2D profiles. **b,c**, Relative phase map $\varphi_{LU}(x, y)$ and content imbalance $s(x, y)$ (at $t = 2.7$ ps). The superimposed lines (red, blue) represent the orbit of photonic vortex cores along the first Rabi cycle after the second pulse arrival (time range $t = 2.7$ – 3.5 ps). One clearly observes their rotation around the two relative phase singularities, specifically around the two LP-mode vortex cores. The asymmetry manifests itself both in the fact that the UP mode cores are more distant from each other than the two LP cores, and that the displacement lines of sight are mutually oblique.

Full-time model

The understanding of the motion mechanics is provided by the toy-model which allows to achieve most of the dynamics upon starting with the overlap of LG beams in the normal modes and let them evolve due to the differential decay and the Rabi oscillations. A more complete coupled Schrödinger equations model would allow to further achieve the initial transient dynamics during the second pulse arrival. Compared to the unitary vortex case[20], the situation is more complicated because the underlying texture of the relative phase is now shaped as a vortex quadrupole (versus a vortex dipole in the case of a single vortex). The configuration of the four poles impressed in the relative phase after the second pulse arrival can be that of a square, a rectangle, a rhombus or a parallelogram. In fact, depending on the relative strength and phase delay between the two pulses, all such different initial situations can be realised. Experimentally there are two effects to be considered. One is that the initial LG_{02} pulse has always a small LG_{00} component (due to imperfect tuning of the q-plate or other residual intensity) and the first pulse then imprints in the polariton fluid to two vortices which are not ideally overlapped and centered, but with a slight preliminary offset in opposite directions with respect to the center of the beam. Then, the arrival of the second pulse is inducing a further displacement which may indeed happen along the same direction or a different one, and this displacement can also differ for the LP and UP vortex cores. A second factor is that upon the arrival of the second pulse, the differential decay of the modes has altered the amplitudes ratio between the two modes, with respect to the one imprinted by pulse. The lesser content is that of the UP (as this mode decays faster), which makes this mode more sensitive to the displacement induced by the second pulse. As a matter of fact, it can be seen in Fig. 4b that the UP cores are more offset than the LP ones with respect to the center. Nevertheless, the initial situation after the two pulses can in general be taken into account by a four LG models, one LG_{02} and one LG_{00} in both of the modes, with the same center and widths σ but with different amplitudes and phases. The initial displacement of the two cores inside each mode is then symmetric, but the direction and amount of such displacement is different for the LP and UP modes. A typical scenario is reproduced in Fig. 5a where the more asymmetric condition of the four poles making a parallelogram is represented (corresponding to the experimental case). The vortex quadrupole is shown together with the relative phase and imbalance isolines, and further superimposed the vortices cores trajectories. Interestingly, even if the imbalance isolines ($s(x, y) = \text{const}$) are not circles, they are still

perpendicular to the relative phase isolines ($\hat{s} \perp \hat{\varphi}_{LU}$). This is due to the initialization by two centered LG beams of the same size σ, independently from their winding numbers. In the case when the LGs are displaced, this feature is lost[27]. In other terms, the Bloch sphere's parallels and meridians that are by definition orthogonal on the sphere surface, remain mutually orthogonal in real space, and likewise any other angle relation is preserved, meaning that the mapping between the Bloch sphere of polariton states and the real space is a conformal mapping. However, it cannot be simply described by a homeomorphism as in a single Rabi-oscillating vortex case[20], since the one-to-one link is lost (each polariton state is mapped twice to the real space).

The evolution of the polariton imbalance map $s(x, y)$ is shown in Fig. 5b. The initially closed orbits ($s = 0$, white loop regions in the first small panel) expand until when, approximately at the moment of the global populations balance, they become two diagonal edge lines connecting each other at infinite distance[28], and start to shrink again, into a single 8-shaped line. After that, they detouch in the central point leaving two closed orbits again. The moving cores can end up their spiral in one or the other of the two final orbits, depending on which side they are immediately before the moment of the detouching (which is set by the initial conditions and γ_{LU}/Ω_R ratio). This crossing possibility is also expressed by the central point being a saddle point[29], which means that the relative phase is defined but its isolines have a singularity in their direction. Due to the conformal feature, the same is also valid for the imbalance isolines. A full view of the orbit line evolution in time is presented in Fig. 5c, depicted as two different perspectives for the sake of clarity, with the central point visible as a 3D saddle point of the $s = 0$ surface (opposite concavities along different transverse directions in the xyt domain).

Berry curvature and its reshaping

It is interesting to note that the density of the relative phase and imbalance isolines in space is described by the so-called Berry curvature. Indeed, associating to the polariton state the pseudospin vector on the Bloch sphere and looking for its dependence in real space, one can express the Berry curvature as

$$B_z = \frac{1}{2}\sin\theta(\partial_x\theta\partial_y\varphi_{LU} - \partial_y\theta\partial_x\varphi_{LU}). \qquad (1)$$

The Berry curvature is describing how much area of the Bloch sphere is covered when spanning a given area segment in real space, also linking the full-wavefunction densities between the two spaces. For objects considered here (*i.e.*, doubly spiraling vortices), the Berry curvature assumes the shape of a double peak in most of the cases, see Fig. 5d. The time dynamics shows these peaks drifting from the initial positions on top of the two UP vortex cores to the positions of the two LP cores. However, in a more symmetric case, such that with orthogonal displacements between the UP and LP vortex

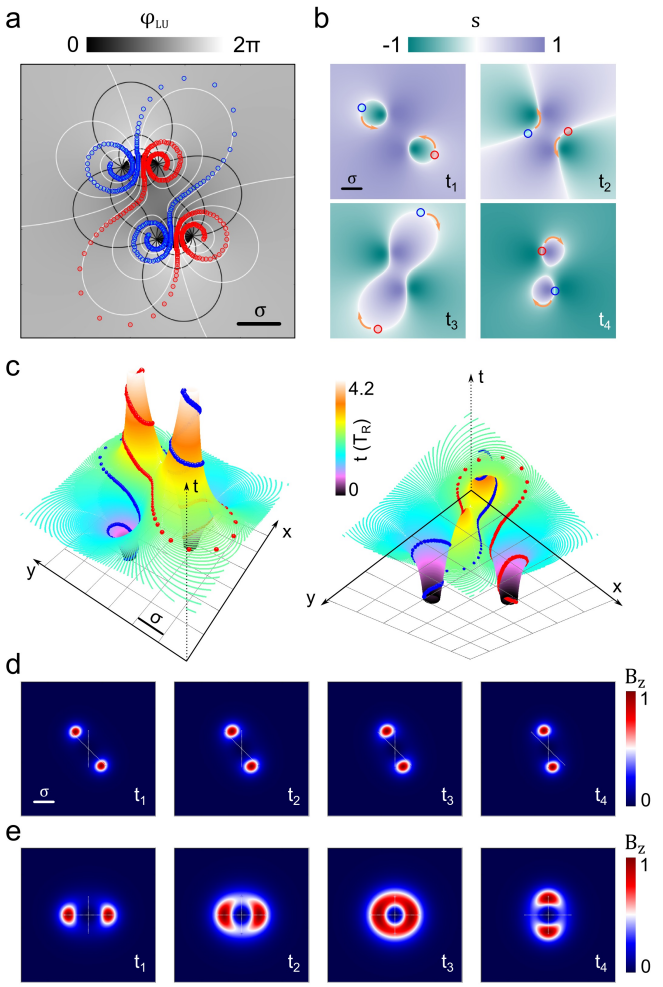

Fig. 5. Model double vortex spiraling. a, The quadrupole relative phase φ_{LU} (black and white map) when starting with a larger UP content. The trajectory of the vortex cores in the photonic field is tracked (blue and red open circles) at isospaced times. The black solid lines are isolines of relative phase (every 30°), the white solid lines are isolines of content imbalance (from 0.8 to -0.8 with the step 0.2). **b**, Maps of the normal modes imbalance $s(x, y)$ at different times, with its reshaping due to the differential decay (which also results in changing of the global content imbalance). The instantaneous orbits of the photon vortex cores follow the white contour lines ($s = 0$), with the two charges motion schematically marked with the red and blue circles. Two initial orbits expand till they join at infinity, then become an eight-shaped line until they finally recoil into two separated petals again. **c**, Perspective views of the isocontent $s = 0$ line evolving in time, drawing a 3D surface with two valleys and two hills. The early/bottom cones open out from the position of the UP vortex cores, the later/upper cones wrap into the position of the LP cores. The overlapped spheres mark the photon vortex cores trajectory. Under different situations (e.g., decay to Rabi-splitting ratio), the cores would start spiraling in before getting close to the central saddle point, and the vortex lines wrap around the opposite LP cone. **d**, Normalized Berry curvature map in the same case as in previous panels and for the same time frames as in panel b. **e**, Normalized Berry curvature map in the case of orthogonal displacements between the UP and LP vortex pairs, at the same times as in panels b,d. The two dashed white lines in d,e mark the UP and LP vortex pairs line of sight. The spatial integral of the Berry curvature is 8π in both d,e and at any time. See also the Supplementary movie SM2.

pairs (achievable upon proper phase delay), the Berry curvature assumes the shape of a ring at intermediate times (approximately at the moment of the two populations balance), as shown in Fig. 5e. The two maxima however effectively become diverging curvature points when the global population imbalance is prevalently in one of the two modes, *i.e.*, when initializing the system at the UP mode energy or always, at long times, when the differential decay leads to a mainly LP content. For example, if considering the stereographic projection linking the Bloch sphere to real space in the case of unitary vortex beams[20], such a singular point emerges as the limit of the sphere contracting to a zero radius. We have verified that for both the experimental case and the two model cases, the entire space integral of the Berry curvature is 8π (twice the solid angle, or half of it if considering the ½ prefactor), due to the two-fold symmetry of the mapping, and it is such at any time despite their reshaping, further confirming these states as dynamical double full Bloch beams.

Discussion

Our experiments demonstrate that it is possible to realize double cores vortex configurations and set them into a peculiar spiraling dynamics, powering the mechanism by use of the Rabi oscillations or any analogue kind of normal modes interference. Such structuring schemes can be interesting, e.g., in the field of complex light, or for driving atomic condensates or other optical tweezers. Eventually such a scheme could be applied to irregular or regular multiple charges such as vortex lattices, and could also be transposed to any (mechanical, acoustic, electronic) platform of 2D coupled oscillators. The localization of the moving vortex cores, thanks to their dip in intensity could allow a more macroscopic observable for detectors such as Doppler gyroscopes. The varying vortex cores displacement from the centre also offers a nice visualization of what is happening to the wavefunction in the case of time-varying OAM, recently drawn to the attention[20,30] in different physical realizations. Behind this there is the concept that the mean OAM per particle is not directly identified by the presence of a given number of vortices for general beams (superpositions of angular-momentum eigenstates)[31,32], but it depends on their positions and the surrounding density shape (despite each vortex can independently exert a torque close to its core). The variety of dynamical and generic full Bloch beams offers the possibility to investigate all such concepts, with their mathematical links to topological textures and the deeper meaning of entities such as the Berry curvature.

Acknowledgements. We would like to thank Romuald Houdré and Alberto Bramati for the microcavity sample, Lorenzo Marrucci and Bruno Piccirillo for the q-plate devices, and sir Michael V. Berry for interesting comments. We acknoweldge for funding the Russian Foundation for Basic Research (joint with CNR, Project No. 20–52–7816); Ministero dell'Istruzione, dell'Università e della Ricerca (PRIN project InPhoPol); Ministero dell'Istruzione, dell'Università e della Ricerca (CUP: B83B17000010001, delibera CIPE n. 3449 del 7/08/2017, FISR MIUR CNR, TECNOMED); Regione Puglia (CUP: B84I18000540002, DGR n. 2117 del 21/11/2018, TecnoMed Puglia); Iran National Science Foundation (97009377).

Supplementary Movie SM1. Experimental Rabi-oscillating double vortex seen in the photonic component as in Fig. 1. Photonic amplitude and phase in a 100×100 μm^2 area, with 20 fs time step over a 4.20 ps time span. The second photonic pulse is arriving at around $t = 2.4$ ps. The vortex cores positions are marked with yellow dots and circles in the amplitude and phase maps.

Supplementary Movie SM2. The LGs model for the double Rabi-oscillating vortex, comprising the maps and dynamics of four relevant quantities. The four panels show the local imbalance $s(\boldsymbol{r},t)$ (purple-green map) and the relative phase $\varphi_{LU}(\boldsymbol{r},t)$ (black and white map) on the top row, as in Fig. 5a,b, together with the photon and exciton densities $|\psi_{\mathrm{C,X}}(\boldsymbol{r},t)|$ (blue and red maps, respectively) in the second row. The positions of the displaced UP/LP cores are corresponding to the poles of the vortex quadrupole in the relative phase map. The spiraling motion of the photon and exciton cores, seen as holes in their respective fields, are tracked by the crossing points between the $s = 0$ isocontent (white) and the $\varphi_{LU} = 0$ and $\varphi_{LU} = \pi$ isophase lines (black lines).

REFERENCES

[1] E. Hodby, S. A. Hopkins, G. Hechenblaikner, N. L. Smith, and C. J. Foot, *Experimental Observation of a Superfluid Gyroscope in a Dilute Bose-Einstein Condensate*, Phys. Rev. Lett. **91**, 090403 (2003).

[2] D. C. Aveline, J. R. Williams, E. R. Elliott, C. Dutenhoffer, J. R. Kellogg, J. M. Kohel, N. E. Lay, K. Oudrhiri, R. F. Shotwell, N. Yu, and R. J. Thompson, *Observation of Bose–Einstein condensates in an Earth-orbiting research lab*, Nature **582**, 193 (2020).

[3] W. Thomson, *4. On Vortex Atoms*, Proc. R. Soc. Edinburgh **6**, 94 (1869).

[4] A. Karch and D. Tong, *Particle-Vortex Duality from 3D Bosonization*, Phys. Rev. X **6**, 031043 (2016).

[5] H. J. Zhao, V. R. Misko, J. Tempere, and F. Nori, *Pattern formation in vortex matter with pinning and frustrated intervortex interactions*, Phys. Rev. B **95**, 104519 (2017).

[6] L. Dominici, R. Carretero-González, A. Gianfrate, J. Cuevas-Maraver, A. S. Rodrigues, D. J. Frantzeskakis, G. Lerario, D. Ballarini, M. De Giorgi, G. Gigli, P. G. Kevrekidis, and D. Sanvitto, *Interactions and scattering of quantum vortices in a polariton fluid*, Nat. Commun. **9**, 1467 (2018).

[7] J. Leach, M. R. Dennis, J. Courtial, and M. J. Padgett, *Vortex knots in light*, New J. Phys. **7**, 55 (2005).

[8] M. R. Dennis, R. P. King, B. Jack, K. O'Holleran, and M. J. Padgett, *Isolated optical vortex knots*, Nat. Phys. **6**, 118 (2010).

[9] J. F. Nye and M. V. Berry, *Dislocations in Wave Trains*, Proc. Roy. Soc. A **336**, 165 (1974).

[10] M. Krenn, J. Handsteiner, M. Fink, R. Fickler, R. Ursin, M. Malik, and A. Zeilinger, *Twisted light transmission over 143 km*, Proc. Natl. Acad. Sci. **113**, 13648 (2016).

[11] Y. Yan, G. Xie, M. P. J. Lavery, H. Huang, N. Ahmed, C. Bao, Y. Ren, Y. Cao, L. Li, Z. Zhao, A. F. Molisch, M. Tur, M. J. Padgett, and A. E. Willner, *High-capacity millimetre-wave communications with orbital angular momentum multiplexing*, Nat. Commun. **5**, 4876 (2014).

[12] G. Gibson, J. Courtial, M. J. Padgett, M. Vasnetsov, V. Pas'ko, S. M. Barnett, and S. Franke-Arnold, *Free-space information transfer using light beams carrying orbital angular momentum*, Opt. Express **12**, 5448 (2004).

[13] H. He, M. E. J. Friese, N. R. Heckenberg, and H. Rubinsztein-Dunlop, *Direct Observation of Transfer of Angular Momentum to Absorptive Particles from a Laser Beam with a Phase Singularity*, Phys. Rev. Lett. **75**, 826 (1995).

[14] A. Forbes, M. de Oliveira, and M. R. Dennis, *Structured light*, Nat. Photon. **15**, 253 (2021).

[15] J. Secor, R. Alfano, and S. Ashrafi, *Complex Light* (IOP Publishing, 2016).

[16] D. Lopez-Mago, *On the overall polarisation properties of Poincaré beams*, J. Opt. **21**, 115605 (2019).

[17] D. Sugic, R. Droop, E. Otte, D. Ehrmanntraut, F. Nori, J. Ruostekoski, C. Denz, and M. R. Dennis, *Particle-like topologies in light*, Nat. Commun. **12**, 6785 (2021).

[18] S. Donati, L. Dominici, G. Dagvadorj, D. Ballarini, M. De Giorgi, A. Bramati, G. Gigli, Y. G. Rubo, M. H. Szymańska, and D. Sanvitto, *Twist of generalized skyrmions and spin vortices in a polariton superfluid*, Proc. Natl. Acad. Sci. **113**, 14926 (2016).

[19] A. M. Beckley, T. G. Brown, and M. A. Alonso, *Full Poincaré beams*, Opt. Express **18**, 10777 (2010).

[20] L. Dominici, D. Colas, A. Gianfrate, A. Rahmani, V. Ardizzone, D. Ballarini, M. De Giorgi, G. Gigli, F. P. Laussy, D. Sanvitto, and N. Voronova, *Full-Bloch beams and ultrafast Rabi-rotating vortices*, Phys. Rev. Res. **3**, 013007 (2021).

[21] T. Byrnes, N. Y. Kim, and Y. Yamamoto, *Exciton–polariton condensates*, Nat. Phys. **10**, 803 (2014).

[22] G. Dagvadorj, J. Fellows, S. Matyjaśkiewicz, F. Marchetti, I. Carusotto, and M. Szymańska, *Nonequilibrium Phase Transition in a Two-Dimensional Driven Open Quantum System*, Phys. Rev. X **5**, 041028 (2015).

[23] L. Dominici, G. Dagvadorj, J. M. Fellows, D. Ballarini, M. D. Giorgi, F. M. Marchetti, B. Piccirillo, L. Marrucci, A. Bramati, G. Gigli, M. H. Szymańska, and D. Sanvitto, *Vortex and half-vortex dynamics in a nonlinear spinor quantum fluid*, Sci. Adv. **1**, e1500807 (2015).

[24] L. Dominici, D. Colas, S. Donati, J. P. Restrepo Cuartas, M. De Giorgi, D. Ballarini, G. Guirales, J. C. López Carreño, A. Bramati, G. Gigli, E. del Valle, F. P. Laussy, and D. Sanvitto, *Ultrafast control and Rabi oscillations of polaritons*, Phys. Rev. Lett. **113**, 226401 (2014).

[25] I. D. Maleev and G. A. Swartzlander, Jr., *Composite optical vortices*, J. Opt. Soc. Am. B **20**, 1169 (2003).

[26] K. Y. Bliokh, M. A. Alonso, and M. R. Dennis, *Geometric phases in 2D and 3D polarized fields: geometrical, dynamical, and topological aspects*, Rep. Prog. Phys. **82**, 122401 (2019).

[27] L. Dominici, N. Voronova, D. Colas, A. Gianfrate, A. Rahmani, V. Ardizzone, D. Ballarini, M. De Giorgi, G. Gigli, F. P. Laussy, and D. Sanvitto, *Shaping the topology of light with a moving Rabi-oscillating vortex*, Opt. Express **29**, 37262 (2021).

[28] G. Molina-Terriza, L. Torner, E. M. Wright, J. J. García-Ripoll, and V. M. Pérez-García, *Vortex revivals with trapped light*, Opt. Lett. **26**, 1601 (2001).

[29] M. V. Berry, in *Second International Conference on Singular Optics (Optical Vortices): Fundamentals and Applications*, Vol. 4403, edited by M. S. Soskin and M. V. Vasnetsov, International Society for Optics and Photonics (SPIE, 2001) pp. 1 – 12.

[30] L. Rego, K. M. Dorney, N. J. Brooks, Q. L. Nguyen, C.-T. Liao, J. San Román, D. E. Couch, A. Liu, E. Pisanty, M. Lewenstein, L. Plaja, H. C. Kapteyn, M. M. Murnane, and C. Hernández-García, *Generation of extreme-ultraviolet beams with time-varying orbital angular momentum*, Science **364**, eaaw9486 (2019).

[31] M. V. Berry, in *International Conference on Singular Optics*, Vol. 3487, edited by M. S. Soskin, International Society for Optics and Photonics (SPIE, 1998) pp. 6–11.

[32] S. Maji, P. Jacob, and M. M. Brundavanam, *Geometric phase and intensity-controlled extrinsic orbital angular momentum of off-axis vortex beams*, Phys. Rev. Appl. **12**, 054053 (2019).

Supplementary Files

This is a list of supplementary files associated with this preprint. Click to download.

- videoS1L2exp.mp4
- videoS2L2modelmaps.mp4